Structure, Stability, Electrochemical and catalytic properties of polyoxometalates immobilized on choline-based hybrid mesoporous silica

Josefa Ortiz-Bustos[a], Yolanda Pérez[a,b]*, Isabel del Hierro[a]*

[a] Departamento de Biología y Geología, Física y Química Inorgánica. Escuela Superior de Ciencias Experimentales y Tecnología. Universidad Rey Juan Carlos. 28933 Móstoles (Madrid), Spain.

[b] Advanced Porous Materials Unit, IMDEA Energy, Av. Ramón de la Sagra 3, 28935 Móstoles, Madrid, Spain.

E-mail: isabel.hierro@urjc.es

Abstract

Polyoxometalate-based heterogeneous catalysts have been prepared by immobilization of Keggin-type heteropolyacid on hybrid mesoporous silica nanoparticles with choline hydroxide based ionic liquid. The immobilization process has been accomplished by a simple acid-base reaction with phosphomolybdic acid. For comparison purposes, additional supports (hybrid-SBA-15 and TiO_2) have been also used in order to establish the nature of the interactions between the heteropolyacid and the surface's groups of the support. To do this, electrochemical and ^{31}P MAS-NMR studies have been carried out finding the formation of moieties like $(Chol)_2[HPMo_{12}O_{40}]$ and/or $(Chol)_3[PMo_{12}O_{40}]$ on the silica materials. Polyoxometalate-based heterogeneous catalysts have been effectively tested for the oxidative desulfurization of DBT in model oil. Thus, complete removal of sulphur (99.7 %) was achieved with polyoxometalate supported on the silica after 2 h and using H_2O_2 as a green oxidant. Additionally, reusability and stability studies of the most active catalyst have been performed.

Keywords: Polyoxometalates immobilized, Mesoporous silica nanoparticles, Heteropolyacid stability, Heterogeneous oxidative desulfurization

1. Introduction

Keggin-type heteropolyacids (HPA) are strong Brönsted acids with interesting redox properties so they have emerged as catalysts and photocatalysts [1, 2] and useful materials in energy storage or in the production of biomass [3]. To increase the chances of Keggin-type heteropolyacids as efficient heterogeneous catalysts the accessibility of the active sites must be improved. That is protons, which act as Brönsted acid; oxygen atoms that are basic enough to abstract protons from organic substrates and metallic active sites. In order to disperse this highly stable species polyoxometalates, mainly phosphotungstic and phosphomolybdic acids, $[H_3PM_{12}O_{40}]$ M = W (HWP) and Mo (HMoP), have been immobilized onto different inorganic supports such as zeolites [4], metallic oxides [5], graphene [6], carbon nanotubes [7], silica [8, 9] and even used as building units in the preparation of metal organic frameworks [10].

In this scenario, mesoporous silica materials with high surface area and high thermal stability are the perfect candidates to be used as supports [11]; nevertheless, the classic impregnation techniques with high HPA loadings achieved high surface coverages and random clusters aggregation onto mesoporous silica surface, which lead to leaching processes during the catalytic reactions in polar solvents. To overcome this drawback an alternative route has been proposed to prepare these hybrid polyoxometalate mesoporous silica materials in a direct synthesis procedure by introducing the HPA in an acidified solution of the surfactant during the synthesis. This methodology allows the encapsulation of HPW anions into SBA-15; however, the final surface structure seems to be highly dependent of the content of HPW finding significant surfaces defects with 30-40 % loadings [4, 12]. The utilization of hybrid organic-inorganic mesoporous silica seems instead a logical proposal as shown by Kaleta and co-workers, who using aminopropyl functionalized MCM-41 material, synthesized a zwitterionic material highly stable and solvent tolerant with strongly immobilized heteropolyanions [13].

The benefits offered by ionic liquids have also been exploited by Li and co-workers who have performed the immobilization of phosphotungstic acid by direct reaction of the heteropolyacid with silica previously functionalized with 1-propyl-3-ethoxysilyl-3-methylimidazolium chloride ionic liquid [14]. Yang and co-workers have used a similar anion interchange reaction to prepare a mesoporous polyoxometalate based polymeric hybrid [15]. Balula and co-workers have recently reported the synthesis of phosphotungstate anion based ionic liquids $[(IL_3)(PW_{12}O_{40})^{3-}]$ (IL = 1-butyl-3-methylimidazolium, 1-butylpyridinium, hexadecylpyridinium) and their application as catalysts in desulfurization of fuel in the presence of 1-butyl-3-methylimidazolium hexafluorophosphate as extractant agent. These biphasic systems seem to be very efficient in the oxidation of sulfur compounds to sulfones but showed a low stability in the recycling process. As an alternative these authors immobilized the phosphotungstate anion onto SBA-15 previously functionalized with N-trimethoxysilylpropyl-N,N,N-trimethylammonium chloride achieving a highly recyclable

catalysts with similar efficiency [16]. Recently, Bryzhin and co-workers have synthesized SILP systems by impregnation of sulfated imidazolium ionic liquids with heteropolyacids (HPA) as anions onto silica and alumina. The hydrogen bonding formation between thiophene and sulfated cation distorted the planar structure and the aromaticity of thiophene. The synergistic effect of this distortion with the catalytic oxidation function of heteropolyanion makes the thiophene activation more efficient [17].

The nature of the interaction, ionic or covalent, between the support and the cluster has great influence on their properties. The bonding between the polyoxometalate molecule (POM) and the silica surface may take place via the formation of hydrogen bonds between the acidic protons of heteropolyacids and the surface silanol groups which can occur with or without proton transfer from POM molecule to the surface silanol groups. A second alternative is the formation of covalent bonds between POM oxygen and surface silicon atoms by water release [18]. Lefebvre and co-workers [19] have demonstrated that, employing classical impregnation procedures, the protons of polyoxometalates interact with surface silanol in silica [$\equiv Si(OH...H)^+$] consuming the three acidic protons and changing the properties of polyoxometalates. However, when the impregnation is performed using anhydrous heteropolyacids and partially dehydroxylated silica, it is possible to obtain well-distributed and well-defined surface species being the main one $[\equiv Si(OH...H^+)]_2[H^+][PMo_{12}O_{40}]^{3-}$. In these types of metallic complexes, the protons of the heteropolyacids are displaced around the structure to optimize the interaction with the silica, establishing strong hydrogen bonds with available silanol groups, but they are not transferred to the silanol group and remain on the polyoxometalate to give structures of the type $\equiv Si\text{-}OH \cdots H^+\text{-}O\text{-}Mo$.

In this work, making use of similar procedures based on organometallic surface chemistry strategies, we have immobilized phosphomolybdic acid ($H_3PMo_{12}O_{40}$) by using dried ethanol as solvent and dehydrated hybrid silica mesoporous nanoparticles. The mesoporous silica nanospheres functionalized with choline hydroxide based ionic liquid, previously prepared by our group [20], allow the immobilization of the Keggin-type heteropolyacid by a straight acid-base reaction with the acid protons of the heteropolyacid. In addition, the lower density of silanol groups available on the silica surface of this material (dehydroxylated before functionalization) should guarantee the stability of the structure and the preservation of the acid protons on the surface. Meanwhile preparing this work, Zeng and co-workers have recently published the synthesis of choline-phosphotungstic acid; the electronic excited state analysis of this material has demonstrated that the formation of singlet oxygen $^1O_2$ is related to the electron hole interaction in the photocatalytic process of ground state molecular oxygen activation. Subsequently this system has reported as an useful photocatalyst in desulfurization of fuel with air and acetonitrile [21]. The aim of this work is to get further information about the influence of the silica surface silanol groups on the tethered heteropolyacid stability, that is why two additional supports have been chosen for

comparison purposes, mesoporous silica SBA-15 functionalized with the choline hydroxide ionic liquid functionality and masked silanol groups and mesoporous titania since it has demonstrated to preserve the phosphomolybdate anion after its supporting [22].

2. Experimental

2.1. Materials

The following reactants were acquired from Merck and used as received: tetraethylortosilicate (TEOS) 98 %, poly(ethylene glycol)-block-poly(propylene glycol)-block-poly(ethylene glycol) (Pluronic P123), trimethylamine (4.2 M in ethanol), hexamethyldisilazane (HMDS), 3-glycidyloxypropyl)trimethoxysilane, sodium hydroxide, hydrogen peroxide solution 30 % (H_2O_2) and dibenzothiophene. Hexadecyltrimethylammonium bromide (CTBA) and phosphomolybdic acid solution (20 % ethanol) were purchased from Acros Organics and used as received. Dodecane ≥ 99.8 % was acquired from Alfa Aesar, 2-propanol from VWR Chemicals and n-octane from Fluorochem. Nitric and hydrochloric acids were purchased from Scharlau. Toluene, dichloromethane and ethanol were purchased from SDS and distilled and dried from appropriate drying agents.

2.2. Preparation of catalysts

2.2.1. Preparation of mesoporous silica nanoparticles (MSN) functionalized with choline hydroxide ionic liquid by post-synthesis procedure (Chol-MSN)

The mesoporous silica nanoparticles (MSN) were synthesized according to previously published procedures [23]. Then, 2 g of MSN were dehydrated during 16 h at 200 °C and then were suspended in 30 mL of dried toluene with 4 mmol of 3-(glycidyloxypropyl)trimethoxysilane and heated at 85 °C for 48 h. After that, the solid was filtered, washed with dichloromethane, and dried under vacuum. In a second step, the previously prepared Gly-MSN material was suspended in water and 4 mmol of a solution of trimethylamine 4.2 M in ethanol was added. The mixture was stirred at 50 °C for 48 h. Finally, the white solid, Chol-MSN, were filtered, washed with dichloromethane and ethanol, and dried under vacuum.

2.2.2. Functionalization of Chol-MSN with phosphomolybdic acid (POMs-Chol-MSN)

0.5 g of Chol-MSN was suspended in 30 mL of ethanol and different amounts of phosphomolybdic acid (0.2-0.5 mmol) was added. The yellow mixture was dispersed in ethanol and stirred for 2 h in a cold bath. After that, the yellow solid was recovered by filtration and washed with dichloromethane. For its storage, the catalyst was dried under vacuum. The obtained samples were named POMs(1-3)-Chol-MSN depending on the amount of phosphomolybdic acid used as reactant (see Table 1).

2.2.3. Functionalization of Chol-HMDS-SBA-15 with phosphomolybdic acid (POMs-Chol-HMDS-SBA-15)

The mesoporous silica material Chol-HMDS-SBA-15 was prepared according to previously published method [20] and functionalized with phosphomolybdic acid following a similar procedure to that of section 2.2.2.

2.2.4. Functionalization of TiO_2 nanoparticles with phosphomolybdic acid (POMs-TiO_2)

The mesoporous TiO_2 nanoparticles were prepared using a procedure described by our group previously [24]. 0.5 g of TiO_2 nanoparticles were suspended in ethanol (30 mL) and 0.2 mmol of phosphomolybdic acid were added. The yellow mixture was stirred during 2 h in a cold bath and then, the solid was filtered and washed with dichloromethane. The resulting solid (POMs-TiO_2) was dried under vacuum.

2.3. Characterization

X-Ray diffraction (XRD) patterns of the materials were obtained on a Phillips Diffractometer model PW3040/00 X'Pert MPD/MRD at 45 KV and 40 mA, with Cu-Kα radiation (λ=1.5418 Å). The adsorption-desorption isotherms of N_2 gas were acquired using a Micromeritics TriStar 3000 analyser, and based on the adsorption branch, pore size distributions were calculated using the Barret- Joyner-Halenda (BJH) model. Thermogravimetric analysis was done in a Star System Mettler Thermobalance and Infrared spectra were recorded on a Nicolet-550 FT-IR spectrophotometer (in the region 4000 to 400 cm^{-1}) as KBr disks. ^1H NMR spectra were recorded on a Varian Mercury FT-400 spectrometer. Structural characterization was completed via transmission electron microscopy (TEM) in a PHILIPS TECNAI-10 electronic microscope operated at 200 kV. The electrochemical studies were recorded with a potentiostat/galvanostat Autolab PGSTAT302 through modified carbon paste electrodes (MCPE) used as working electrode, as in previous studies reported by our group [23].

2.4. Oxidative desulfurization

For this experiment, 50 mg of catalyst, 10 mL of n-octane as model oil containing DBT (250 ppm S) and 30 % H_2O_2 (O/S =6) were added in a reactor MultiMax™ parallel reactor system from Mettler Toledo. The mixture was heated at (40-60 °C) at different times and stirred at 500 rpm. After that, the solid was separated by centrifugation and the supernatant was analyzed to calculate the remaining sulfur content by GC-FID (Agilent 6890N, DB-Wax capillary column 25 m, 0.53 mm) using dodecane as an external standard. The resulting product was dibenzothiophene sulfone and it was also identified by liquid ^1H NMR spectroscopy (Fig. S11). The catalysts were washed with dichloromethane and dried under vacuum. The catalyst POMs(2)-Chol-MSN was used in repeated experiments with the aim to prove its recycling.

3. Results and discussion

3.1. Synthesis and Characterization of catalysts

Mesoporous silica nanoparticles with the functionality choline hydroxide has been synthesized previously by our group [20]. This functionality act as strong base allowing the straightforward acid-base reaction with phosphomolybdic acid in organic media to render immobilized polyoxometalates (POMs), which establish electrostatic interactions with ammonium groups covalently grafted to silica surface. This strategy aims to produce well-distributed and well-defined surface species, where the protons remaining in the molybdenum cluster can be displaced around the structure and may establish hydrogen bonds with the hydroxyl group available in the choline type tethered ligand (See Scheme 1), or in less extension with the surface silanol groups. In addition, the masked of silanol groups with hexamethyldisilazane in the material Chol-HMDS-SBA-15 will not be capable of establishing strong hydrogen bonds with surface silanol and hence the transference of the proton acid from the heteropolyacid to give additional Mo-O-Si covalent bonds. For comparative purposes, mesoporous TiO_2 supported phosphomolybdic acid has been also used since titanium oxide has demonstrated to preserve the phosphomolybdate anion after its immobilization [22, 25].

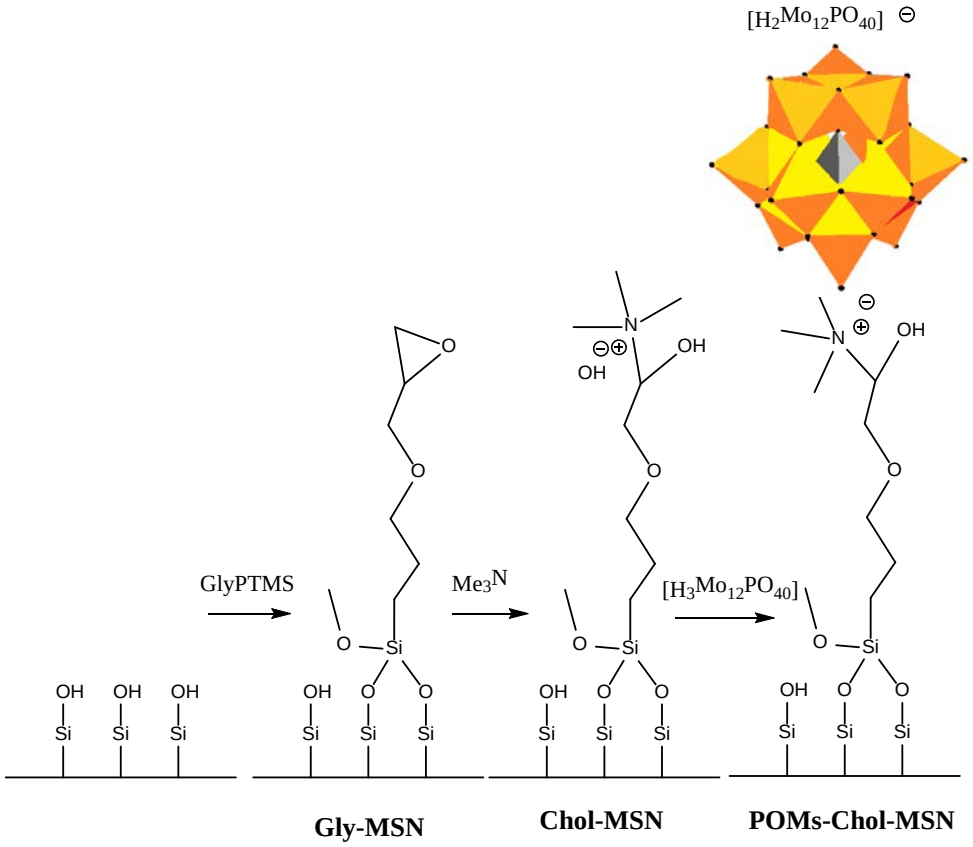

GlyPTMS = 3-glycidyloxypropyl)trimethoxysilane

Scheme 1. Immobilization procedure of Keggin-type phosphomolybdic acid or polyoxometalates (POMs) onto hybrid mesoporous nanospheres.

To study the loading capacity of the materials synthesized in this work, several amounts of phosphomolybdic acid as POMs metallic precursor have been used. The phosphomolybdic acid content was calculated based on X-ray fluorescence analysis (XRF). As can be seen in Table 1, three samples with increasing amount of phosphomolybdic acid (mmol/g) in the modified MSN nanoparticles have been obtained besides those prepared with Chol-HMDS-SBA-15 and TiO_2 as supports. POMs-Chol-MSN and POMs-Chol-HMDS-SBA-15 samples show higher quantities of phosphomolybdic acid in their surfaces than POMs-TiO_2 which only contains 0.05 mmol g^{-1}. Fig. S1a and Fig. 1 show the nitrogen adsorption/desorption isotherms of pristine supports and functionalized materials, respectively. The POMs-Chol-HMDS-SBA-15 material shows a characteristic type IV BET isotherm due to the presence of mesoscale pores with a characteristic H1-type adsorption-desorption hysteresis loop of a highly ordered hexagonal pore system. This type of isotherm is also shown by POMs-TiO_2 sample, but its hysteresis loop is a mixture of H1 and H2 from 0.4 to 0.9 relative pressure, which is typical of these mesoporous aggregates of TiO_2 nanoparticles [24]. As representative example of hybrid POMs mesoporous silica nanoparticle materials, POMs(2)-Chol-MSN sample has a type III isotherm with a H1 hysteresis loop centered at $P/P_0 > 0.9$. The textural properties such as the surface area (S_{BET}), total pore volume (V_p) and BJH pore diameter (D_p) have been obtained from N_2 isotherms (Table 1 and Fig. S1b). The modified SBA-15 material possesses expected values for S_{BET} (183.2 $m^2 g^{-1}$), V_p (0.25 $cm^3 g^{-1}$) and D_p (4.8 nm) when the support has been functionalized with choline ionic functionality and a silylating agent, like HMDS [20]. The POMs-TiO_2 mesoporous nanoparticles possess lower values of surface area (80.4 $m^2 g^{-1}$), pore volume (0.18 $cm^3 g^{-1}$) and pore diameter (7.0 nm) with respect to non-modified TiO_2 nanoparticles after phosphomolybdic acid incorporation, as befitted. The three materials POMs-Chol-MSN show an important reduction in the textural properties' values in comparison with the bare MSN. The high loading value of choline moieties and sterically demanding phosphomolybdate anions support its incorporation into the channels and hence the blocking of nitrogen molecules entrance, as the XRD patterns suggest. With the values of POMs loading (L_o = % Mo/(12×molybdenum atomic weight) and S_{BET} of the samples, we also calculate the average surface density of attached POMs molecules and the average intermolecular distance. As expected, the modified MSN samples have the lowest surface density in the range 0.08-0.13 molec/nm^2 and higher intermolecular distance from 0.53 to 0.76 nm. POMs-Chol-HMDS-SBA-15 shows 0.22 molec/nm^2 and an intermolecular distance of 2.12 nm. In the same way, both parameters calculated for POMs-TiO_2 are 0.24 molecules/nm^2 of average surface density and 2.05 nm of intermolecular distance. Finally, to assess the extent of the ion pair formation between the tetra alkyl ammonium group and the polyoxometalate counter ion, the ratio between POMs, and the choline based ligand has been estimated in POMs-Chol-HMDS-SBA-15 and POMs(2)-Chol-MSN samples. Since the choline ligand loadings calculated from nitrogen elemental analysis measurements are 0.64 y 0.81 mmol/g for Chol-HMDS-

SBA-15 and Chol-MSN; the ratio POMs/Choline ligand are 0.4 and 0.3, respectively. These low values are consistent with the formation of complexes like $(Chol)_2[HPMo_{12}O_{40}]$ and/or $(Chol)_3[PMo_{12}O_{40}]$ besides the presence of unreacted choline hydroxide units onto the silica surface cannot be discarded. This proposal offers new variables to be considered during the characterization and application of these materials.

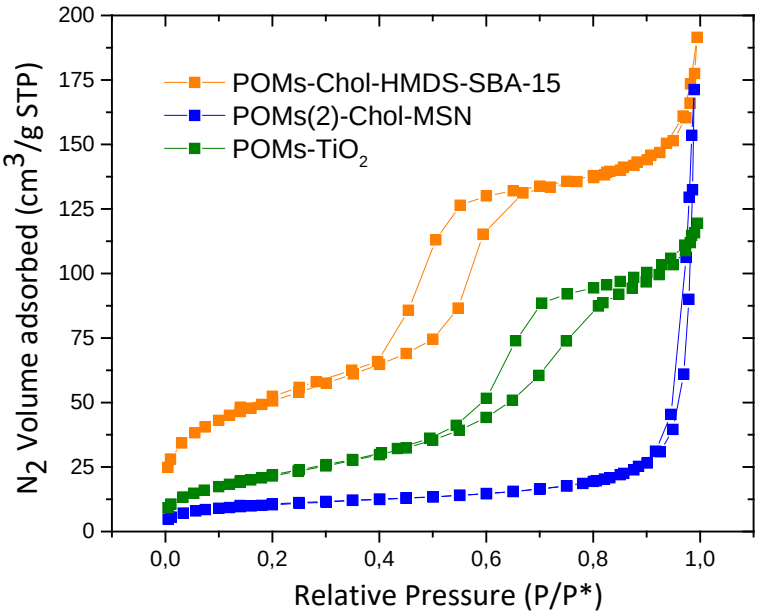

Figure 1. N_2 adsorption/desorption isotherms of some functionalized samples.

Table 1. Textural properties, phosphomolybdic acid loading, average surface density, average intermolecular distance and band gap values of the synthesized materials.

Material	S_{BET} (m^2g^{-1})	Pore Volume (cm^3g^{-1})	Pore size (nm)	Phosphomolybdic acid loading (L_o) (mmol g^{-1})[a]	Average surface density (molecules/nm^2)	Average intermolecular distance (nm)	Band Gap (E_g)[c]
MSN	1024	0.97	2.77	-	-	-	-
POMs(1)-Chol-MSN	35.1	0.17	1.4	0.22	0.13	2.80	2.73
POMs(2)-Chol-MSN	37.5	0.27	2.4	0.21	0.12	2.90	2.74
POMs(3)-Chol-MSN	50.4	0.23	2.4	0.14	0.08	3.46	2.63
POMs-Chol-HMDS-SBA-15	183.2	0.25	4.8	0.25	0.22	2.12	2.80
TiO_2	84.6	0.19	8.1	-	-	-	3.15
POMs-TiO_2	80.4	0.18	7.0	0.05	0.24	2.05	3.07
POMs (in ethanol)	-	-	-	-	-	-	2.98

[a] The molybdenum content was obtained by X-ray fluorescence analysis (XRF). (L_o = % Mo×10/(12×molybdenum atomic weight)

[b] Blue shifted value calculated for Mo=O_t and Mo-O-Mo transition bands after immobilization in comparison to free POMs in ethanolic solution

[c] Estimated band-gap energy (E_g) from a plot of $(\alpha h\nu)^2$ *vs* $h\nu$

The mesostructure of the synthesized silica-based materials was investigated by XRD analysis (Fig. 2a). Small-angle XRD studies show that pristine MSN material has a typical well-resolved pattern at low 2θ values with three characteristic peaks: one strong (100) at 2.44 and two lower (110) and (200) at 4.1 and 4.8 (Fig. 2a), respectively; corresponding to a highly ordered mesoporous silica. This structure has also been confirmed by SEM and TEM micrographs (Fig. S2). The hybrid Chol-MSN material containing the organic functionality suffers a pronounced reduction in the main peak intensity at 2.44 and the peaks (110) and (200) disappear, as well as the POMs-Chol-MSN samples. The intensity´s decrease on the diffraction plane (100) can be explained by changes in the wall thickness due to the ongoing functionalization process on nanoparticles surface and the likely blocking of pores as the N_2 adsorption analysis suggests. Thus, the unit cell parameter, $a_0 = 2d_{100} \times (\sqrt{3})^{-1}$, was calculated considering d_{100} values. MSN, Chol-MSN and POMs-Chol-MSN samples possess increasing a_0 values of 4.16, 4.35 and 4.39 nm, respectively, which means an increment in the distance between two contiguous pores in that crystallographic direction (d_{100}). The XRD pattern of POMs-TiO_2 sample was also performed showing its crystalline nature (Fig. 2b). Although anatase phase (A) is the main crystal phase additional peaks of brookite phase (B) appeared at 2θ = 31 and 42, due to the low calcination temperature (400 °C) used during the experimental synthetic procedure for the crystalline structure formation. Wide XRD studies for POMs-Chol-MSN and POMs-Chol-HMDS-SBA-15, as well as, POMs-TiO_2 materials do not show peaks attributed to crystalline POMs which supports the uniform dispersion of the polyoxometalate anions onto silica materials (Fig. S3). In addition, there is no measurable effect on the size of the titanium oxide nanoparticles upon clusters immobilization as demonstrate de average particle diameter for both TiO_2 and POMs calculated to be about 7.6 nm by using Scherrer's formula.

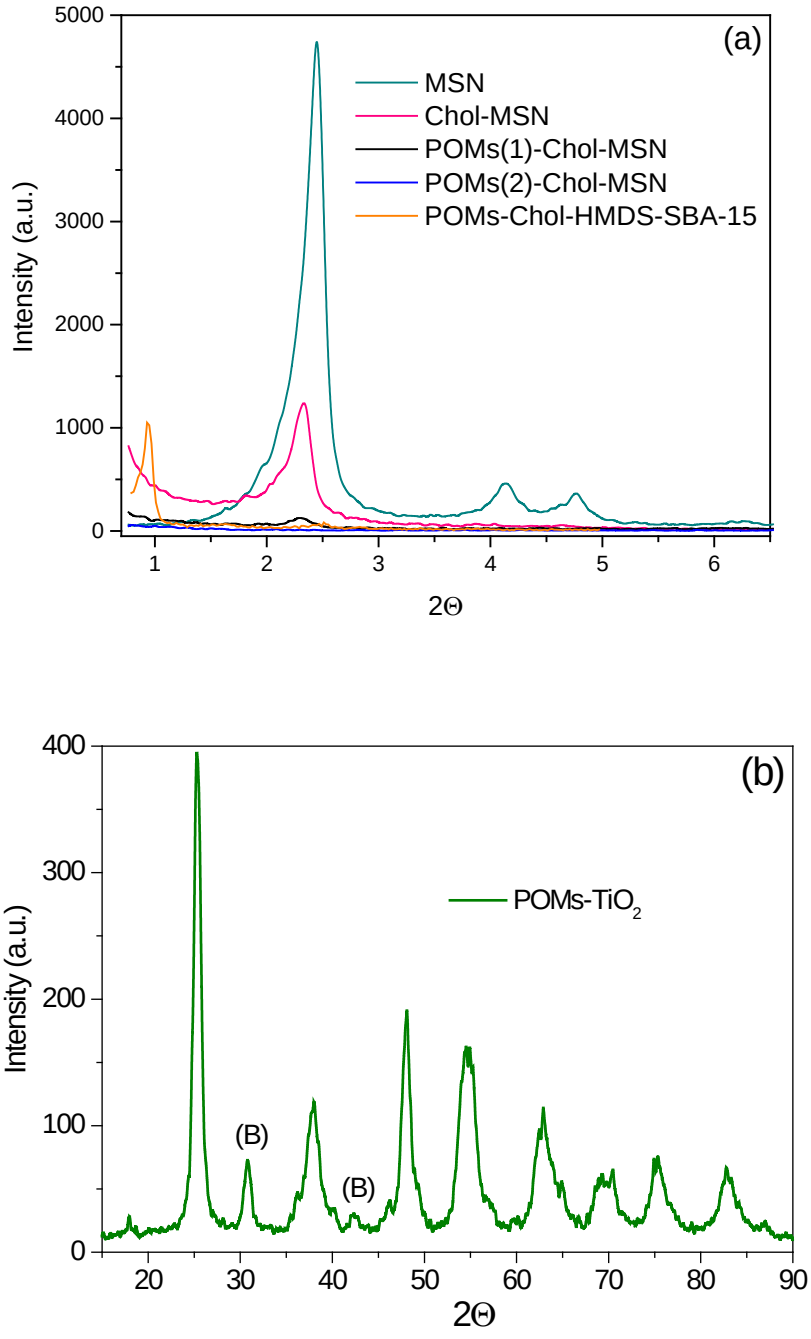

Figure 2. XRD patterns of a) bare and modified MSN and SBA-15 materials and b) POMs-TiO_2 sample.

The thermal behavior of POMs-Chol-MSN and POMs-Chol-HMDS-SBA-15 was studied by thermogravimetric and differential thermal analysis (TGA and DTA). TGA curve of POMs-Chol-MSN, in Fig. 3, exhibits a small weight loss around 100 °C due to physisorbed water on surface´s samples. Then, a weight loss region is found from 160 to 400 °C corresponding to decomposition of organic moiety anchored to surface silica and a sharp peak is located at 500 °C associated to phosphomolybdic acid decomposition. Pure

[$H_3Mo_{12}PO_{40}$] decomposes at ca. 440 ºC, that is, phosphomolybdic acid maintains a similar thermal stability after immobilization in Chol-MSN. This behavior contrasts with that observed for [$H_3Mo_{12}PO_{40}$] loosely anchored on silica or on montmorillonite which is less stable than unsupported [26]. New exothermic peaks at 755 and 845 ºC are observed in the DTA curves; these peaks are ascribed to additional decomposition of POMs to render MoO_3. POMs-Chol-HMDS-SBA-15 material shows a similar TGA curve with subtle differences, the broad peak in the range 185-380 ºC now, which involves the decomposition of choline-based ligand and that of trimethylsilyl groups anchored to the silica surface, Me_3Si-O-Si≡. Besides, the first peak attributed to the decomposition of POMs appears at lower value ca. 465 ºC in comparison to POMs-Chol-MSN. The slight increase of POMs decomposition in POMs-Chol-MSN suggests, besides, the accepted electrostatic interactions with the choline-based functionality, the establishment of an additional interaction between polyoxometalate anions and unmasked silanol groups which are capable of further stabilization of supported POMs.

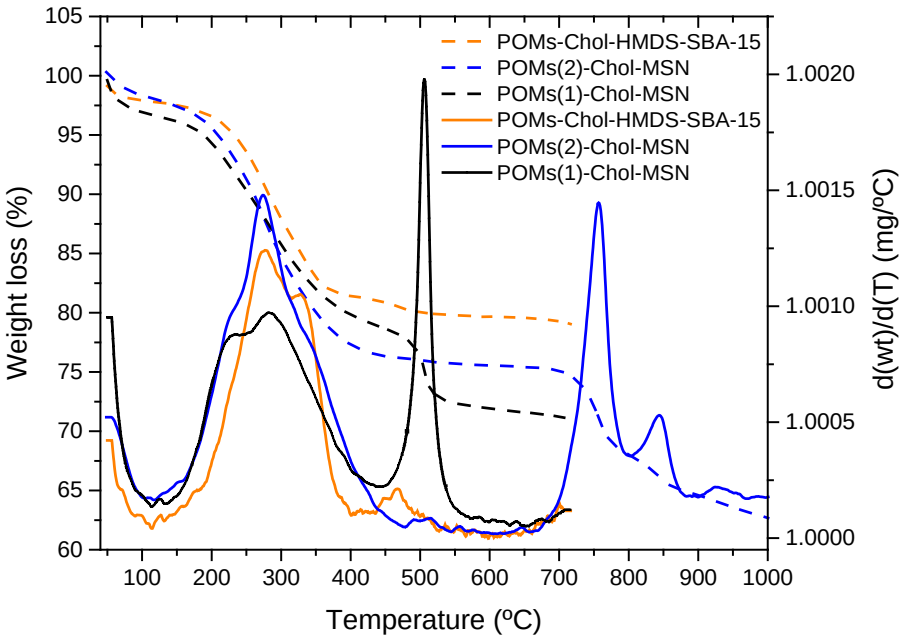

Figure 3. TGA and DTA analysis curves for POMs-Chol-MSN and POMs-Chol-HMDS-SBA-15 materials.

Fig. 4 and Fig. S4 show the FTIR spectra of synthesized materials. The characteristic bands of the physisorbed water molecules appear at 3432 cm^{-1} and at 1637 cm^{-1} corresponding to O-H stretching and deformation vibrations, respectively. Silica-based materials show other typical sharp bands attributed to the Si-O stretching vibrations at 1086, 962 and 808 cm^{-1} (Fig. S4). The incorporation of choline ionic liquid adds new bands to the spectra corresponding to ν(C-H) stretching vibrations at 2937 and 2881 cm^{-1} and two nearby bands at 1476 and 1487 cm^{-1} attributed to the bending vibrations of

δ(C-H) of the tetraalkyl ammonium group of the choline unit (Fig. S4). These bands remain unaltered after phosphomolybdic acid incorporation, which support the stability of these organic functionality. For comparison purposes, the FTIR spectrum of pure phosphomolybdic acid ($H_3PMo_{12}O_{40}$, 20 % ethanol) was also recorded (Fig. 4a). Keggin-type $H_3PMo_{12}O_{40}$ is formed by assembly of MoO_6 octahedral sharing edge oxygen atoms to form units which further condense by sharing corner oxygen atom around a phosphorus central atom in tetrahedral coordination (PO_4) surrounded by 12 MoO_6 octahedral to form the cage structure. There are four central oxygen atoms (P-O_a), 12 oxygen atoms that bridge two molybdenum atoms sharing a central oxygen atom (O_c), 12 oxygen atoms that bridge molybdenum atoms not sharing a central oxygen atom and 12 terminal oxygen atoms bound to a single molybdenum atom (O_b). FTIR spectrum of $H_3PMo_{12}O_{40}$ is dominated by four characteristic peaks at 1046, 963, 882 and 810 cm^{-1}, assigned to the ν(P-O_a), ν(Mo=O_t) (O_t is terminal oxygen), ν(Mo-O_b-Mo) (O_b is bridge oxygen) and ν(Mo-O_c-Mo) (O_c is the corner or edge oxygen), respectively. In POMs mesoporous silica-based materials with variable loading of phosphomolybdic acid (Fig. 4a), the most representative bands due to the polyoxometalate units appear overlapped by the intense stretching vibration of hybrid silica support. It is probable that the interaction of the POMs subunits, well dispersed on silica surface, with unmasked silanol groups cause the distortion of the symmetry and hence the decrease and broadening of the bands. This fact is supported by the FTIR spectrum of POMs-Chol-HMDS-SBA-15 (Fig. 4b) where the bands assigned to Mo–O_b–Mo and Mo–O_c–Mo are clearly observed and appear slightly shifted to 885 and 805 cm^{-1} in comparison to unsupported $H_3PMo_{12}O_{40}$, which indicates the maintenance of the symmetry of the Keggin-type structure upon immobilization and partial replacement of acid protons by the choline-based cation. FTIR spectrum of POMs-TiO_2 material, synthesized by direct incorporation of phosphomolybdic acid onto mesoporous titanium oxide nanoparticles, shows bands at 1045, 960 and 805 cm^{-1} (Fig. 4b). The band assigned to the external oxygen atoms ν(Mo-O_b-Mo) shows an important decrease which again indicates the decrease of symmetry due to the strong affinity between anions and surface groups of support meanwhile maintaining the Keggin-type structure.

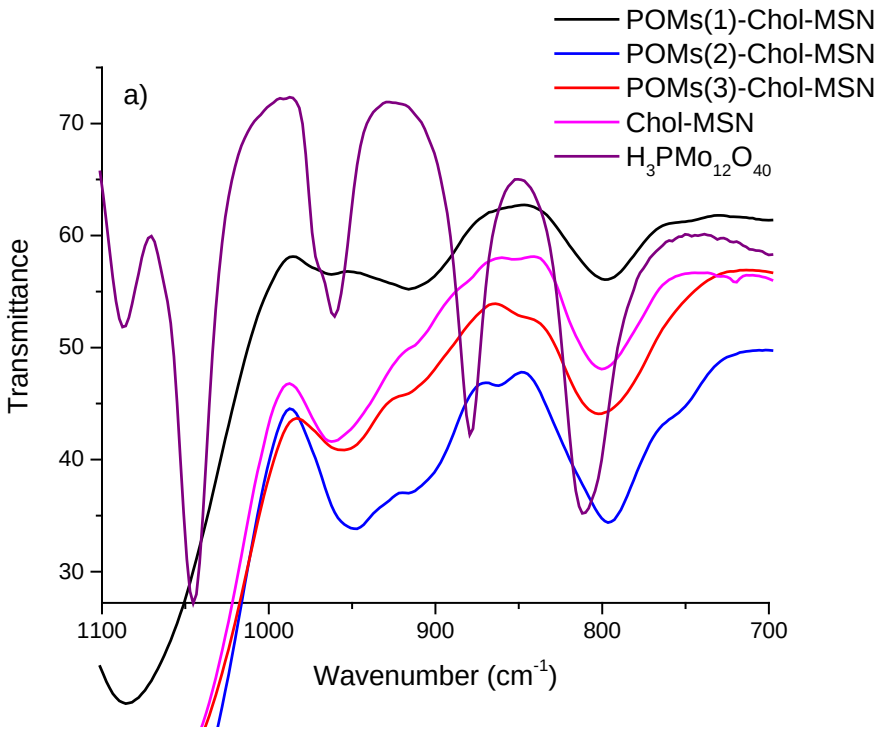

1

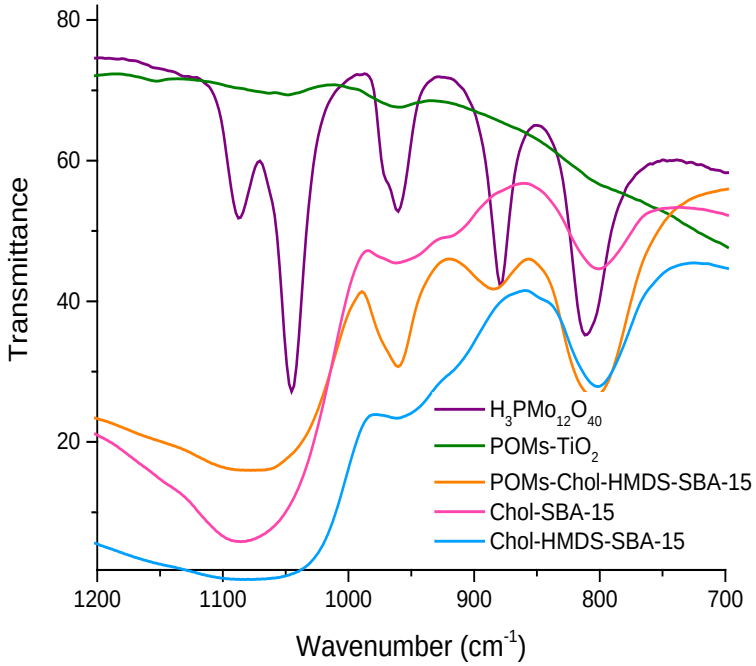

2

3 Figure 4. FTIR spectra of POMs hybrid materials synthesized in this work in comparison
4 to phosphomolybdic acid.

5 To obtain further conclusions about the electronic structure, the existence of anion-
6 anion interactions and anion-support interactions, UV–vis measurements were
7 performed. The diffusion reflectance ultraviolet visible absorption spectra of

synthesized materials are shown in Fig. 5. As can be seen, two strong signals appear in all samples in the ranges of 220-240 nm and 305-317 nm. The reflectance band between 220-240 nm is attributed to ligand-metal charge transfer (LMCT) transition of terminal oxygen to molybdenum atoms ($Mo=O_t$). The band located at 305-317 nm corresponds to the presence of Mo-O-Mo bridges and the transition type LMCT between bridging oxygen atoms and molybdenum [27]. These signals are characteristic of phosphomolybdic acid, as can be verified in Fig. S5a, where the UV–vis spectrum of an ethanolic solution of $H_3PMo_{12}O_{40}$ at 0.05 mg mL^{-1} concentration was recorded. Both bands display red shifted after immobilization and proton substitution by the choline based counterion with exception of the spectrum of POMs(3)-Chol-MSN material where appear slightly blue shifted. It can be said that the red shifted observed for $O^{2-} \rightarrow Mo^{6+}$ is proportional to the amount of supported POMs in POMs-Chol-MSN materials (see Table 1) and hence can be related not only to the immobilization but mainly to the relative distance between anions, so the lower molecular distance the higher is the displacement. In fact, in the compound $(Chol)_3[PW_{12}O_{40}]$ recently reported, the proton replacement by the large cation involves a clear blue shift [21]. The shift observed is similar for the absorption peaks due to $Mo=O_t$ and Mo-O-Mo transition bands indicating that terminal and bridged oxygen-molybdenum bonds are equally affected after immobilization on these materials. In comparison, the absorption spectrum recorded for POMs-Chol-HMDS-SBA-15 offers interesting characteristics; the band due to terminal metal-oxygen bond, $Mo=O_t$, appears blue shifted contrary to what could be expected considering that this material possesses the lowest calculated average molecular distance. In addition, the peak at 305 nm attributed to Mo-O-Mo appears at the lowest wavenumber measured in all the materials under study. Edge energies calculated for LMCT transitions from Kubelka–Munk plots are clearly dependent on the relative distance between molecules and hence on anion-anion interactions. The values, for all of them, are below the calculated value of 2.98 eV for $H_3PMo_{12}O_{40}$ in ethanol and decrease with the molecular distance increase. POMs-Chol-HMDS-SBA-15 is the material with the highest value of band gap (2.80 eV) that also possesses the lowest relative molecular distance. For POMs-TiO_2, the edge band calculation is mainly due to the anatase phase and it is not possible to infer clear conclusions. These results suggest that exist an influence of several factors in the DRUV-Vis bands position of Keggin-type phosphomolybdic acid after immobilization, such as the bulky counterion of the polyoxometalate anion present in all materials (except POMs-TiO_2), the anion-anion interactions and the surface-anion interactions.

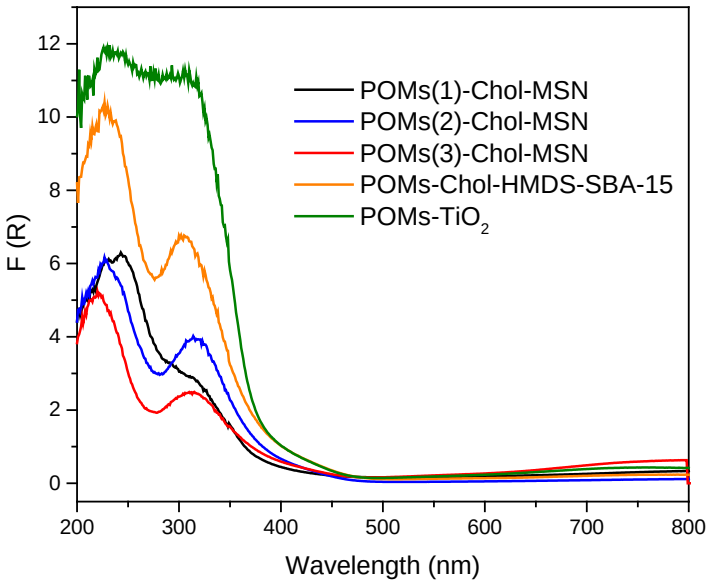

Figure 5. DRUV-Vis spectra of POMs based materials synthesized in this work.

^{31}P MAS-NMR is a very sensitive technique to local phosphorus chemical environment and surrounding symmetry. Thus, this technique can add extra information to characterize changes in chemical environment, after polyoxometalate was supported on the provided support. The ^{31}P MAS-NMR spectrum of POMs(2)-Chol-MSN immobilized on OH^- exchanged choline MSN material (Fig. 6) shows three sharp resonances at δ -6.9 -4.8 and -0.26 ppm, indicating three different possible phosphorous environments. Since the samples have been always treated and stored under nitrogen atmosphere and dried ethanol used as solvent in synthetic procedures, the existence of multiple signals cannot be explained on the basis of a different degree of hydration, as Black and co-workers did for the ^{31}P MAS-NMR spectra of $K_3[PMo_{12}O_{40}]$ and $[H_3PMo_{12}O_{40}]\cdot nH_2O$ [28]. Pacula and co-workers [26] explained the presence of two broad signals at −2.7 and −4.9 ppm in the ^{31}P MAS-NMR spectrum of $H_3PMo_{12}O_{40}$ deposited on Na-exchanged montmorillonite due to the formation of $(SiOH_2)^+[H_2PMo_{12}O_{40}]$ or $Na[H_2PMo_{12}O_{40}]$ and further decomposition into $[PMo_{11}O_{39}]^{7-}$ and $[P_2Mo_{18}O_{62}]^{6-}$ anions, because of the alkaline nature of the support. According to Zeng and co-workers [29] pure $H_3PMo_{12}O_{40}$ shows a single signals at δ = −3.33 and $H_3PMo_{12}O_{40}$-SiO_2 a broad resonance due to the overlap of this signal and a weak shoulder at δ = −4.09 ppm attributed to $[(SiOH_2)^+(H_2PMo_{12}O_{40})^-]$. This and similar studies suggest that primary structure of polyoxometalate anion is only weakly perturbed on silica. Nevertheless, in the literature studies with remarkably different results are also available. For instance, Chang and co-workers reported ^{31}P MAS-NMR studies of $H_3PMo_{12}O_{40}$-SiO_2 with different loadings which displays three resonance peaks at 2.5 −3.6 and −10.0 ppm, assigned from high to low fields to decomposition species, pure $H_3PMo_{12}O_{40}$ and interacting species with SiO_2 support [30]. When using more basic supports as alumina up field in the range -8 to -23 ppm peaks

are observed. These signals are explained based on Keggin-type anion decomposition to render monomeric phosphate, polyphosphate and $AlPO_4$ or P_2O_5–MoO_3 complexes with alumina according to Say Prasad [31] or seldom Caceres and co-workers [32] due to the presence of the Keggin-type unit at δ = −3.33 ppm and to the interacting species of phosphomolybdic acid with the support at δ = −10.8 ppm. The ammonium salt of 12-molybdophosphoric acid impregnated on silica at 5 wt% shows only a sharp single peak at 0.0 ppm. On increasing the loading, the peak moved up-field, with enhanced bandwidth extending up to −12 ppm due to the formation of interacting species [31].

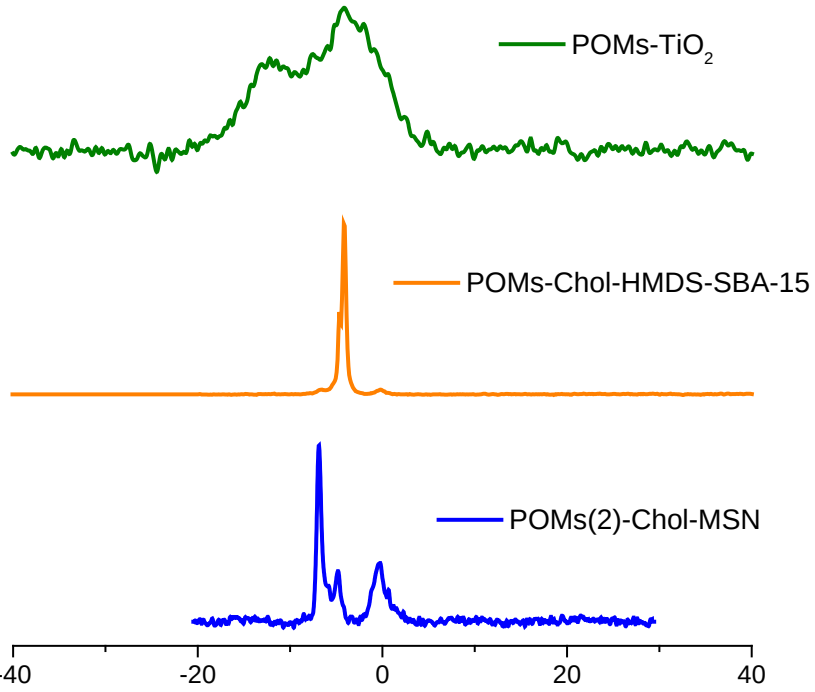

Figure 6. ^{31}P MAS-NMR magnetic angle spinning resonance of POMs based materials synthesized in this work.

The wide range of chemical shifts found in the literature and their plausible explanations evidence the great influence of the support, the metallic precursor and the immobilization procedure. Taking these considerations into account, the measured spectrum for POMs(2)-Chol-MSN in Fig. 6 is consistent with the presence of Keggin-type anions $(Chol)_2[HPMo_{12}O_{40}]$ and/or $(Chol)_3[PMo_{12}O_{40}]$ at δ -6.9 ppm which may further interact with the silica surface -4.8 to give $(\equiv Si\text{-}OH_2)^+_n$–$[(Chol)_{3-n}Mo_{12}PO_{40}]^{n-3}$. In addition, the third peak at δ -0.26 ppm is tentatively assigned to the anion $[PMo_{11}O_{39}]^{7-}$ produced by decomposition of polyphosphomolybdate anions. It is well known that the degradation of polyoxometalates anions takes place in aqueous solutions when the pH value increases. $[H_3PMo_{12}O_{40}]$ in aqueous solution undergoes decomposition at pH > 1 which is visually accompanied by the color change of the solution from yellow to green

to light blue. The solid samples synthetized in this work by using a support with basic properties have been prepared in ethanol solutions which in principle should stabilize such anions; however, these materials show a slight blue color. DRUV-Vis studies do not support depolymerization or decomposition of polyphosphomolybdate anions in great extension, but ^{31}P NMR spectrum of POMs(2)-Chol-MSN points out that the lacunar anion $[PMo_{11}O_{39}]^{7-}$ may be present as indicate the existence of the down shift peak at -0.26 ppm. This lacunar anion may be stabilized as tetraalkylammonium salts whose stability has been previously reported. On the contrary, the ^{31}P MAS-NMR spectrum recorded for POMs-Chol-HMDS-SBA-15 material only shows one peak at δ = –4.11 ppm and a weak shoulder at δ = −4.66 ppm attributed to $(Chol)_2[HPMo_{12}O_{40}]$ and/or $(Chol)_3[PMo_{12}O_{40}]$ immobilized by electrostatic interactions and to $[(SiOH_2)^+(H_2PMo_{12}O_{40})^-]$ formed by hydrogen bond formation with -OH group of the choline base functionality. The absence of surface acid silanol groups predetermines clearly the pattern obtained in the ^{31}P MAS-NMR spectra. In addition, when using a support with surface acid properties as titania, where the hydrolytic decomposition of $[PMo_{12}O_{40}]^{3-}$ is insignificant, the ^{31}P MAS-NMR spectra of POMs-TiO_2 (Fig. 6) displays two broad phosphorus resonance peaks, which indicates that the catalyst exists in two different phases, a major peak at −4.2 ppm and a smaller broad peak at −12.3 ppm. The enhance bandwidth and the upfield shift indicates that the Keggin units greatly interact with titanium oxide support. The study performed by Caceres and co-workers [33] shows that ^{31}P NMR spectra of $H_3PMo_{12}O_{40}$ impregnated TiO_2 samples with different loadings by using ethanol–water, and subsequently dried or calcined display one sharp peak in the range -3.51 to -4.1 ppm, demonstrating the stability of the Keggin-type anion which remains undegraded after immobilization.

Since POMs exhibit rich electrochemistry, we have performed solid state electrochemical studies in acidic media of $H_3PMo_{12}O_{40}$ acid attached to the walls of hybrid mesoporous silica materials. As representative materials POMs(2)-Chol-MSN, POMs-Chol-HMDS-SBA-15 and POMs-TiO_2 have been studied (Fig. 7 and Fig. S7). To do so, modified glassy carbon electrodes were prepared with a mixture of graphite and the material under study and used as working electrode vs an Ag/AgCl/KCl (3 M) reference electrode and a platinum rod as counter electrode. Firstly, cyclic voltammogram of POMs(2)-Chol-MSN shows two quasi reversible two electron consecutive waves at 0.36 and 0.19 V and a third one irreversible at -0.047 V involving more than two electrons as can be inferred from the important increase in the peak height (See Fig. 7a). These redox processes correspond to the reduction of Mo (VI) and are accompanied by the uptake of protons to prevent build-up of negative charge according to the reaction: $[PMo^{VI}_{12}O_{40}]^{3-} + ne^- + nH^+ \rightarrow [H_nPMo^{V}_{n}Mo^{VI}_{12-n}O_{40}]^{3-}$ (n = 2,4,6). For comparison purposes, the electrochemical behavior of phosphomolybdic acid was also study under similar experimental conditions (acidic solution, H_2SO_4 0.5 M) (Fig. S6a). The CV measured is comparable to that of POMs(2)-Chol-MSN, it shows two quasi reversible positive two electron redox reactions at 0.39 and 0.22 V and a third irreversible redox

process at -0.02 V. The appearance of this third irreversible peak, in both CV measured, is interpreted in terms of the hydrolysis of the reactant which involves more than two electrons. This is a very well-known behavior of Keggin-type phosphomolybdates in aqueous electrolytes where it is difficult to obtain well defined redox waves due to easy hydrolysis of $[PMo^{VI}_{12}O_{40}]^{3-}$.

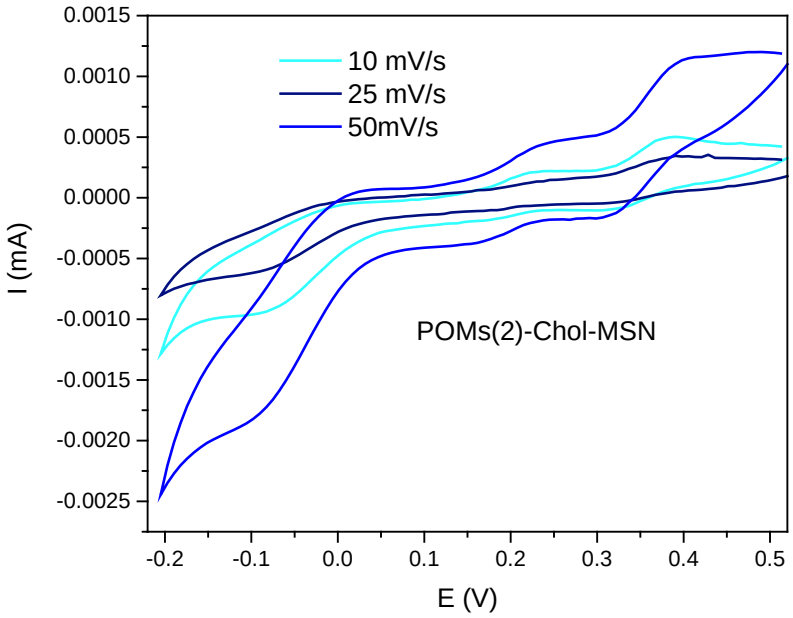

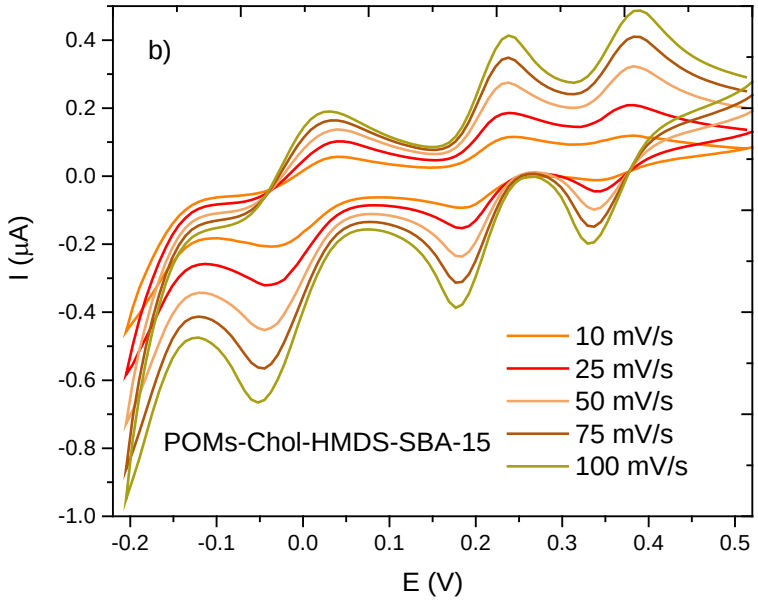

Figure 7. Cyclic voltammograms of a) POMs(2)-Chol-MSN and b) POMs-Chol-HMDS-SBA-15 immobilized on a carbon modified electrode as working electrode in nitrogen

saturated aqueous 0.5 M H_2SO_4 *vs* an Ag/AgCl/KCl (3 M) reference electrode and a platinum rod as counter electrode.

Under similar experimental conditions the material POMs-Chol-HMDS-SBA-15 (Fig. 7b) with non-reactive hydrophobic trimethylsilyl groups on the silica surface exhibits three quasi-reversible redox peaks in the potential range of −200 to 500 mV with half-wave potentials $E_{1/2}$ =(E_{pa}+E_{pc})/2 of 0.36, 0.21 and 0.0 V, respectively; and with a ratio of forward and back peaks slightly deviate from unity Ip_c/Ip_a <1. The peak potentials change gradually following the scan rates, the cathodic peak potentials shift towards the negative direction and the corresponding anodic peak potentials to the positive direction with increasing scan rates. This common phenomenon results from the electron exchange rate between the electrode and the $[PMo_{12}O_{40}]^{3-}$ anions. Plots of current peaks of three cathodic and anodic waves versus scan speed square root show a linear behavior pointing out that the kinetics of the overall process was controlled by diffusion. This behaviour suggests the electrochemical stabilization of the anion probably due to the lack of interactions with the protected silanol groups on the silica surface. Previous studies in organic solvents solutions show similar CV results, for instance, in ethanol $[PMo^{VI}_{12}O_{40}]^{3-}$ undergoes four reversible reductions of two, two, two and four electrons followed by an irreversible two-electron reduction step [34]. When studying the potential values obtained in the above cyclic voltammograms, we observe the first cathodic peak (first reduction) at 0.305 and 0.335 V *vs* Ag/AgCl for POMs(2)-Chol-MSN and POMs-Chol-HMDS-SBA-15, respectively. Meanwhile the measured value for $H_3PMo_{12}O_{40}$ in acidic solution is 0.336 V. A quantifiable shift of 31 mV is measured for the first reduction peak for POMs(2)-Chol-MSN in comparison to $H_3PMo_{12}O_{40}$; this shift to lower reduction potentials (less positive) indicates that the supported POMs molecules in this material are less oxidizing (their oxidation power is lower) than POMs in solution. The experimental results obtained from CV are quite different for POMs-Chol-HMDS-SBA-15 being negligible the shift of the first reduction peak potential in comparison to free $H_3PMo_{12}O_{40}$. Since the organic functionality and immobilization procedure is the same for both materials it seems plausible again that the nature of the surface groups influences greatly the reduction potential of supported POMs.

To go further in this effect, a more sensitive technique as square wave voltammetry was used. Fig. 8 shows the square wave voltammograms (SQWV) of the three materials under study. As can be seen, four cathodic peaks are observed associated to molybdenum reduction processes. SQWV of POMs(2)-Chol-MSN material shows a slight shift to lower potentials in the peak positions in comparison to that POMs-Chol-HMDS-SBA-15, as expected, and negligible changes in the peak heights. On the contrary, the four reduction peaks attributed to POMs-TiO_2 appear at higher potential values (more positive) and the height of the SQWV peaks increases gradually suggesting the involvement of a higher number of electrons in the reduction processes and hence the existence of hydrolysis processes. The SQWV recorded for $H_3PMo_{12}O_{40}$ in solution (Fig.

6b) shows a similar behavior, that is, the structure in solution or immobilized on pristine TiO_2 suffers a severe structure reorganization upon reduction, the absence of any organic functionality makes possible a straight interaction with the reactive groups "Ti-O-H" present in the TiO_2 surface. H^+ is probably delocalized between the anion and the protonated surface $(\equiv Ti\text{-}OH_2)^+_n{-}[H_{3-n}Mo_{12}PO_{40}]^{n-3}$) (See also CV in Fig. S7). The higher potential observed suggests a decrease of the electron density on the POM anion and thus the increase of its oxidizing character.

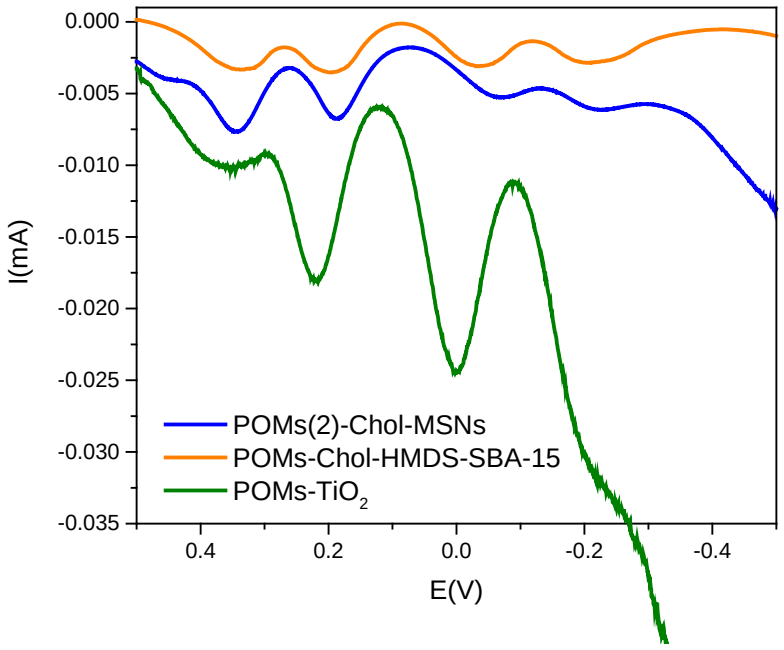

Figure 8. Square wave voltammograms of POMs(2)-Chol-MSN, POMs-Chol-HMDS-SBA-15 and POMs-TiO_2 immobilized on a carbon modified electrode as working electrode in nitrogen saturated aqueous 0.5 M H_2SO_4 vs an Ag/AgCl/KCl (3 M) reference electrode and a platinum rod as counter electrode.

3.2. Oxidative desulfurization of dibenzothiophene (DBT)

3.2.1. Effect of different catalysts on oxidative desulfurization of DBT

Keggin-type heteropolyacids have been widely used as acid catalysts and photocatalysts in many reactions as oxidation, acetylation or dehydration [35, 36], due to their versatile Brønsted acidity and redox powers. Among them, the use of heteropolyacids for oxidizing organic species, under mild reaction conditions, has been the most prominent role [37]. Oxidative desulfurization shows a high efficiency to remove sulfur compounds from petroleum streams and requires neither hard operating conditions nor hydrogen demands [38]. Thus, oxidative desulfurization takes a stance as an approach to ultra-deep desulfurization. In this section, the desulfurization performances of the heterogeneous catalysts prepared in this work were primarily evaluated. Desulfurization experiments were carried out using 10 mL of a DBT solution (250 ppm S) in n-octane, as

model oil, with H_2O_2 as an eco-friendly oxidant, in an O/S ratio of 6 and 50 mg of catalyst and the mixture was maintained for 2 h. The results obtained are listed in Table 2. With the aim to corroborate that the polyoxometalates are the active species in the catalytic process, two blank experiments were primary performed. The first one, without catalyst (Entry 1), with a conversion of DBT of 4.5 % after 2 h, and the second one, with a catalyst modified only with the choline group (Entry 2), in which only 5.1 % of conversion was accomplished.

Table 2. Heterogeneous oxidative desulfurization catalyzed by POM-based heterogeneous catalysts [a].

Entry	Catalyst	PMA loading (L_o) (mmol g^{-1})	Reaction temperature (°C)	Conversion of DBT (%)[b]
1	-	-	60	4.5
2	Chol-MSN	-	60	5.1
3	POMs(1)-Chol-MSN	0.21	60	97.4
4	POMs(2)-Chol-MSN	0.22	60	99.7
5	POMs(3)-Chol-MSN	0.14	60	89.4
6	POMs-Chol-HMDS-SBA-15	0.25	60	99.7
7	POMs-TiO_2	0.05	60	37.2
8	POMs(2)-Chol-MSN	0.22	40	96.2
9	POMs-Chol-HMDS-SBA-15	0.25	40	93.1

[a] Reaction conditions: 50 mg catalyst, molar ratio O/S=6, S-concentration of 250 ppm in n-octane, time: 2 h.

[b] DBT elimination was determined by CG analysis with the external standard method.

In general, the prepared catalysts exhibit remarkably high activities for the removal of DBT under mild oxidation and for 2 h, rendering in all cases the desirable product dibenzothiophene sulfone. At 60 °C, most of the samples shows high conversion values fluctuating between 89.4 % and 99.7 %, except the POMs-TiO_2 sample which reaches 37.2 % of DBT removal (Entry 7). As can be inferred, it exits a correlation between the heteropolyacids loading (L_o) (mmol g^{-1}) and conversion value. Thus, the sample with less amount of polyoxometalates on its surface (POMs-TiO_2) shows the poorest result of conversion. To illustrate the effect of temperature on desulfurization efficiency considering the good obtained results at 60 °C, a decrease in the operation temperature up to 40 °C was set up using the catalysts POMs(2)-Chol-MSN and POMs-Chol-HMDS-

SBA-15, which also obtained high conversions of DBT, 96.2 % and 93.1 %, Respectively (Entries 8 and 9). To optimize the reaction time at 40 °C of temperature, the kinetic of conversion for the POMs(2)-Chol-MSN sample was accomplished at different periods of time and indeed nearly complete oxidation of DBT was obtained at 2 hours (Fig. S8).

The effect of catalyst and H_2O_2 dosage were also investigated at 40 °C (Table 3). Firstly, catalysts were tested at lower ratio O/S = 3 obtaining remarkable conversion values 74.0 % and 84.9 % for POM-Chol-HMDS-SBA-15 and POMs(2)-Chol-MSN catalysts, respectively (Entries 10 and 11). In the latest optimization purpose two oxidation experiments were set up with 25 mg of catalyst and the results were 39.3 % of DBT conversion using POM-Chol-HMDS-SBA-15 catalyst (Entry 12) and 69.2 % with POMs(2)-Chol-MSN (Entry 13). Thus, in these conditions, there are significant differences in catalytic activity between both materials. These major differences could be due to not only to the number of polyoxometalates anchored to surfaces, but also, the average surface density the catalysts have, 0.81 molec/nm^2 the modified SBA-15 support and 3.54 molec/nm^2 the MSN one (see Table 1). As well as, the free and available silanol groups in the MSN surface play an important role for their intrinsic Brønsted acidity [39], which are masked at SBA-15 surface with HMDS as silylating agent. Brønsted acidity of POMs(2)-Chol-MSN material could contribute to the adsorption of DBT and the activation of H_2O_2 promoting the oxidative desulfurization [17].

Table 3. Heterogeneous oxidative desulfurization catalyzed by POM-based heterogeneous catalysts in different conditions [a].

Entry	Catalyst	Molar ratio O/S	Mass of catalyst (mg)	Conversion of DBT (%)[b]
10	POMs-Chol-HMDS-SBA-15	3	50	74.0
11	POMs(2)-Chol-MSN	3	50	84.9
12	POMs-Chol-HMDS-SBA-15	6	25	39.3
13	POMs(2)-Chol-MSN	6	25	69.2

[a] Reaction conditions: 50 or 25 mg catalyst, O/S=6 or O/S=3, S-concentration of 250 ppm in n-octane, time: 2 h, temperature: 40 °C.

[b] DBT elimination was determined by CG analysis with the external standard method.

Similar polyoxometalates-ionic liquids-silica systems have also been recently studied by other groups with some differences in catalysts preparation and catalytic performance. Li et al. [14] grafted 1-propyl-3-triethoxysilyl 3-methylimidazolium chloride in SiO_2 and then immobilized the phosphomolybdate to prepare the hybrid catalyst that was used

in oxidative desulfurization. A complete oxidation of 0.2 %wt (around 250 ppm S) is reached in 90 min at 40 °C, with the best catalyst which has 30 %wt of phosphomolybdic acid loading. Akopyan et al. [40] synthesized series of polyoxometalate-based ionic liquid hybrid materials with high catalytic activity towards DBT and related compounds in short times (1 h), but using acetonitrile as co-solvent and with higher H_2O_2:S ratios (10:1) and temperature (70 °C) than those used in this work. Other recent studies with polyoxometalates as active species used acetic or peroxyacetic acids as co-catalysts, which enhance considerably the conversion due to the easy oxidation of sulfur compounds in acidic media [41, 42].

3.2.2. Reusability of catalyst

To test catalysts' durability and recycling performance, repeated experiments have been conducted in the ODS of DBT for POMs(2)-Chol-MSN under the optimum conditions (50 mg of catalyst, 250 ppm-S, O/S = 6, 40 °C, 2h) and the results are shown in Fig. 10. After each run, the catalyst was filtrated, washed with dichloromethane and dried at 60 °C for 2 h, and then stored under vacuum. The removal of sulfur for the three consecutive runs was satisfactory in terms of sulfone selectivity, exhibiting a slightly drop in the DBT conversion values. To prove the stability of the catalyst, DRUV-Vis and FTIR spectra were recorded and the results show that no significant changes are observed in either of them and that all the characteristic bands and peaks are remaining unaltered before the oxidation reaction (Fig. S9). The result strongly suggests that the polyoxometalate-based mesoporous hybrid materials are durable and recyclable.

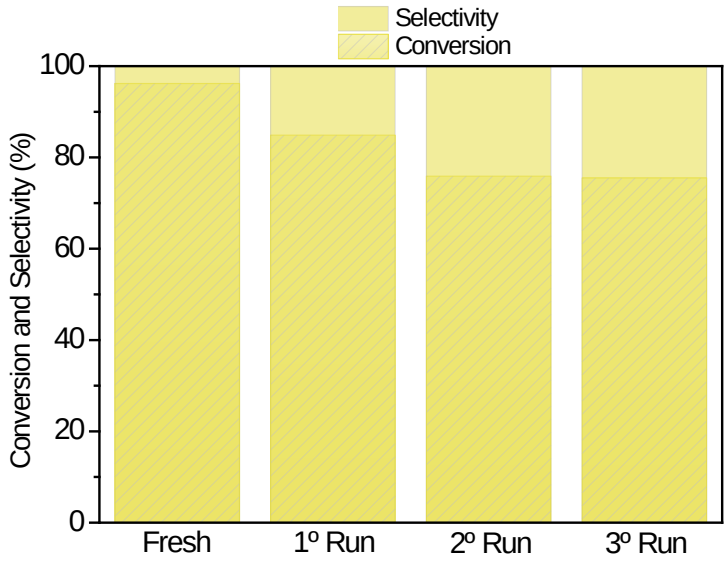

Figure 10. Catalytic activity of POMs(2)-Chol-MSN in consecutive reaction cycles of oxidative desulfurization of DBT.

3.2.3. Stability of POMs(2)-Chol-MSN catalyst

The chemical constitution of the catalyst after the oxidation experiment is confirmed by XPS. For comparison, the starting material is also given. As shown in Fig. 11 the curve of fresh and recycled POMs(2)-Chol-MSN shows Mo 3p, Mo 3d, Si 2s, Si 2p, C 1s, P 3s and O 1s signals are apparently observed from the full survey. Mo3d spectrum of fresh catalyst shows double peaks composed of the 3d5/2 and 3d3/2 levels, resulting from spin– orbit coupling, for Mo^{5+} (232,3 and 235,5 eV) and Mo^{6+} (233.5 and 236.6 eV) being this latter in higher proportion [43]. These findings mean that the main contribution for the Mo reduction comes from the chemical synthesis, Mo^{6+} is converted to Mo^{5+} in the presence of electron donors' groups as Choline functionality and/or surface silanol groups. The surface of the fresh catalyst contains Mo^{6+} and Mo^{5+} species in a 2:1 ratio, meanwhile reused catalyst contains a higher amount of reduced molybdenum species, the Mo^{6+}/Mo^{5+} ratio decreases to 1.5, which can be attributed to the catalytic cycle due to the presence of H_2O_2 and substrate.

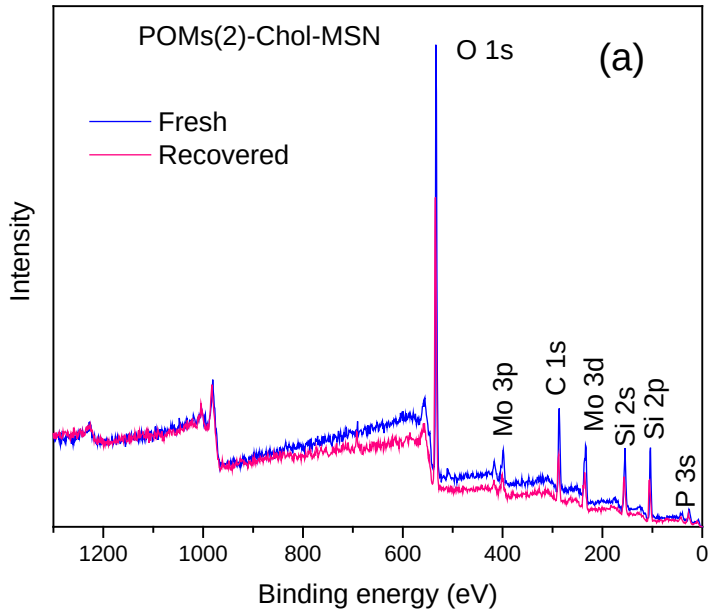
POMs(2)-Chol-MSN
O 1s
(a)
Fresh
Recovered
Intensity
Mo 3p
C 1s
Mo 3d
Si 2s
Si 2p
P 3s
1200
1000
800
600
400
200
0
Binding energy (eV)

1

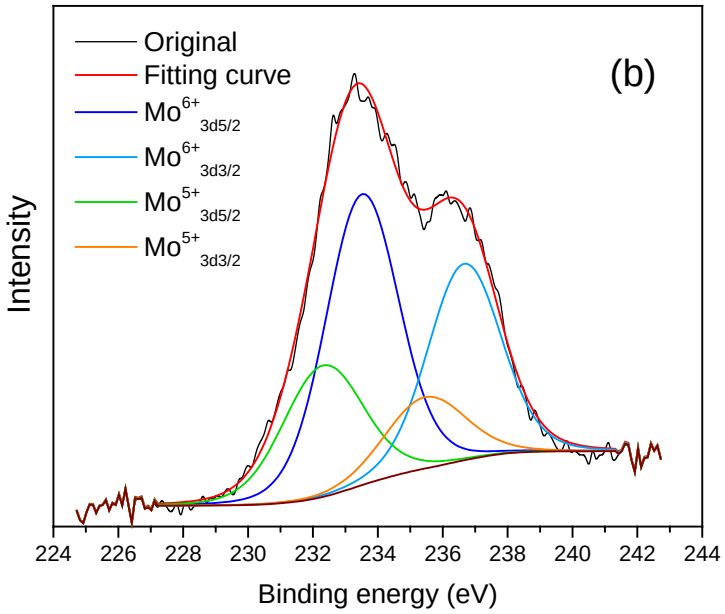
Original
Fitting curve
Mo6+ 3d5/2
Mo6+ 3d3/2
Mo5+ 3d5/2
Mo5+ 3d3/2
(b)
Intensity
224
226
228
230
232
234
236
238
240
242
244
Binding energy (eV)

2

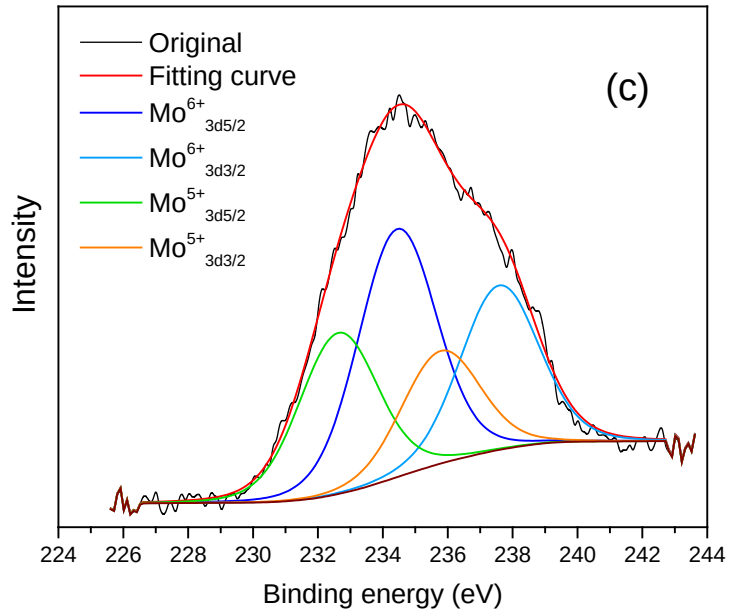

Figure 11. XPS general spectra of (a) fresh and recycled POMs(2)-Chol-MSN. (b) Curve fit of Mo3d spectra of fresh POMs(2)-Chol-MSN (c) Curve fit of Mo3d spectra of recycled POMs(2)-Chol-MSN.

To get an extra insight on the catalyst's stability, electrochemistry studies of carbon paste electrodes modified with POMs(2)-Chol-MSN after H_2O_2 treatment and after the catalysis experiment were performed. We assume the rapid formation of peroxo molybdenum units $Mo(O_2)^{2-}$ after H_2O_2 treatment by reaction of the terminal bond Mo=O of polyoxometalate with hydrogen peroxide to give peroxo groups. Several proposals are found in literature describing the reactivity of polyoxometalates with hydrogen peroxide. Ishii-Venturello chemistry involves the use of heteropolyacids, H_2O_2, and a surfactant that originate a polyoxometalate/H_2O_2 catalytic oxidation system. According to the reaction mechanism proposed, an active peroxo polyoxometalate specie is formed in the aqueous phase by the interaction of the Keggin heteropolyoxometalate with H_2O_2 (Fig. S10). By means of electrochemical studies we want to go further in the nature of the molybdenum species formed by reaction of tethered $(Chol)_2[HPMo_{12}O_{40}]$ and/or $(Chol)_3[PMo_{12}O_{40}]$ moieties with hydrogen peroxide. As can be seen in Fig. 12 after hydrogen peroxide treatment, the voltammogram recorded for POMs(2)-Chol-MSN/H_2O_2 shows four cathodic peaks the same as POMs(2)-Chol-MSN, a slight difference in the first reduction peak is observed, this peak shifts from 0.345 to 0.333 V value indicating higher electron density in the Mo(VI) centers due to the formation of peroxo species. In addition, an important decrease in the peak height is observed for third and fourth reduction steps, which suggests lower stability of the peroxo species formed. After the catalysis experiment, the SQWV for the recovered sample shows significant differences in comparison to fresh

material. The first peak potential appears now at 0.345 V, suggesting the recovery of oxo-species; however, the third and fourth reduction peaks appears overlapped, that is, new Mo=O species have been generated in situ from supported polyoxometalates anions as suggested by the XPS results and according to Venturello mechanism [44-46].

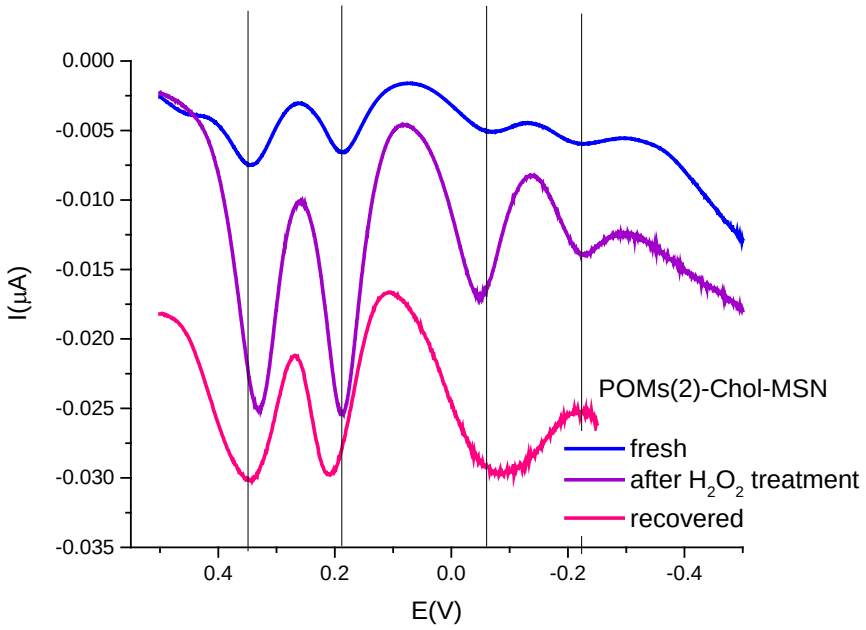

Figure 12. Square wave voltammograms of POMs(2)-Chol-MSN, after H_2O_2 treatment and after recovery essays, immobilized on a carbon modified electrode as working electrode in nitrogen saturated aqueous 0.5 M H_2SO_4 vs an Ag/AgCl/KCl (3 M) reference electrode and a platinum rod as counter electrode.

Conclusion

In this work, heterogenous catalysts with polyoxometalate immobilized onto hybrid silica materials have been prepared and used successfully for ODS system with H_2O_2 as a green oxidant and without co-solvent. Desulfurization test results show that the POM-based heterogeneous catalysts possess high activity due to the presence of polyoxometalates as active species and good reusability due to molybdenum cluster's stability upon immobilization. In fact, all the samples improve its visible light absorption ability after immobilization what enhances their usefulness as photocatalysts. The use of dehydrated hybrid mesoporous silica and surface's organometallic chemistry strategies add new information about the role of silanol groups and their interaction with POM upon immobilization. Electrochemical and ^{31}P MAS-NMR studies concluded that the POMs clusters tethered onto mesoporous silica surface are fully accessible and interact with the surface silanol groups. Thus, silica surface groups play a significant role in the oxidative desulfurization reaction. According to the results, the electronic properties of POMs could be tuned by acting on the nature of the silica surface groups,

when the surfaces become partially dehydroxylated and more hydrophobic less hydrogen bonds are formed between the POM and the surface.

Acknowledgements

We gratefully acknowledge financial support from the MICINN (project RTI2018-094322-B-I00 and CTQ2017-90802-REDT).

References

[1] S.-S. Wang, G.-Y. Yang, Recent Advances in Polyoxometalate-Catalyzed Reactions, Chem. Rev. 115 (2015) 4893-4962.
[2] H.N. Miras, J. Yan, D.-L. Long, L. Cronin, Engineering polyoxometalates with emergent properties, Chem. Soc. Rev., 41 (2012) 7403-7430.
[3] N. Mansir, Y.H. Taufiq-Yap, U. Rashid, I.M. Lokman, Investigation of heterogeneous solid acid catalyst performance on low grade feedstocks for biodiesel production: A review, Energ Convers Manage. 141 (2017) 171-182.
[4] B.C. Gagea, Y. Lorgouilloux, Y. Altintas, P.A. Jacobs, J.A. Martens, Bifunctional conversion of n-decane over HPW heteropoly acid incorporated into SBA-15 during synthesis, J. Catal. 265 (2009) 99-108.
[5] Y. Ren, B. Yue, M. Gu, H. He, Progress of the Application of Mesoporous Silica-Supported Heteropolyacids in Heterogeneous Catalysis and Preparation of Nanostructured Metal Oxides, Materials, 3 (2010) 764-785.
[6] J.-P. Tessonnier, S. Goubert-Renaudin, S. Alia, Y. Yan, M.A. Barteau, Structure, Stability, and Electronic Interactions of Polyoxometalates on Functionalized Graphene Sheets, Langmuir, 29 (2013) 393-402.
[7] Y. Gao, R. Gao, G. Zhang, Y. Zheng, J. Zhao, Oxidative desulfurization of model fuel in the presence of molecular oxygen over polyoxometalate based catalysts supported on carbon nanotubes, Fuel, 224 (2018) 261-270.
[8] J. Alcañiz-Monge, B.E. Bakkali, G. Trautwein, S. Reinoso, Zirconia-supported tungstophosphoric heteropolyacid as heterogeneous acid catalyst for biodiesel production, Appl Catal B-Environ, 224 (2018) 194-203.
[9] S. Zhao, G. Xu, J. Chang, C. Chang, J. Bai, S. Fang, Z. Liu, Direct production of levulinate from carbohydrates catalyzed by H-ZSM-5 supported phosphotungstic acid, BioRes, 10 (2015) 2223-2234.
[10] L.M. Rodriguez Albelo, A.R. Ruiz-Salvador, D.W. Lewis, A. Gómez, P. Mialane, J. Marrot, A. Dolbecq, A. Sampieri, C. Mellot-Draznieks, Zeolitic polyoxometalates metal organic frameworks (Z-POMOF) with imidazole ligands and ε-Keggin ions as building blocks; computational evaluation of hypothetical polymorphs and a synthesis approach, Phys. Chem. Chem. Phys., 12 (2010) 8632-8639.
[11] D. Julião, F. Mirante, S.O. Ribeiro, A.C. Gomes, R. Valença, J.C. Ribeiro, M. Pillinger, B. de Castro, I.S. Gonçalves, S.S. Balula, Deep oxidative desulfurization of diesel fuels using homogeneous and SBA-15-supported peroxophosphotungstate catalysts, Fuel, 241 (2019) 616-624.
[12] P.-Y. Hoo, A.Z. Abdullah, Direct synthesis of mesoporous 12-tungstophosphoric acid SBA-15 catalyst for selective esterification of glycerol and lauric acid to monolaurate, Chem. Eng. J., 250 (2014) 274-287.
[13] W. Kaleta, K. Nowińska, Immobilisation of heteropoly anions in Si-MCM-41 channels by means of chemical bonding to aminosilane groups, Chem Comm, (2001) 535-536.
[14] X. Li, J. Zhang, F. Zhou, Y. Wang, X. Yuan, H. Wang, Oxidative desulfurization of dibenzothiophene and diesel by hydrogen peroxide: Catalysis of H3PMo12O40 immobilized on the ionic liquid modified SiO2, Mol. Catal., 452 (2018) 93-99.

[15] H. Yang, B. Jiang, Y. Sun, L. Zhang, Z. Huang, Z. Sun, N. Yang, Heterogeneous oxidative desulfurization of diesel fuel catalyzed by mesoporous polyoxometallate-based polymeric hybrid, Journal of hazardous materials, 333 (2017) 63-72.
[16] S.O. Ribeiro, B. Duarte, B. De Castro, C.M. Granadeiro, S.S. Balula, Improving the Catalytic Performance of Keggin [PW12O40]3− for Oxidative Desulfurization: Ionic Liquids versus SBA-15 Composite, Materials, 11 (2018) 1196.
[17] A.A. Bryzhin, M.G. Gantman, A.K. Buryak, I.G. Tarkhanova, Brønsted acidic SILP-based catalysts with H3PMo12O40 or H3PW12O40 in the oxidative desulfurization of fuels, Appl Catal B-Environ, 257 (2019) 117938.
[18] X. Rozanska, P. Sautet, F. Delbecq, F. Lefebvre, S. Borshch, H. Chermette, J.-M. Basset, E. Grinenval, Polyoxometalate grafting onto silica: stability diagrams of H3PMo12O40 on {001}, {101}, and {111} β-cristobalite surfaces analyzed by DFT, Phys. Chem. Chem. Phys., 13 (2011) 15955-15959.
[19] E. Grinenval, X. Rozanska, A. Baudouin, E. Berrier, F. Delbecq, P. Sautet, J.-M. Basset, F. Lefebvre, Controlled Interactions between Anhydrous Keggin-Type Heteropolyacids and Silica Support: Preparation and Characterization of Well-Defined Silica-Supported Polyoxometalate Species, J Phys Chem C, 114 (2010) 19024-19034.
[20] I.d. Hierro, Y. Pérez, M. Fajardo, Supported choline hydroxide (ionic liquid) on mesoporous silica as heterogeneous catalyst for Knoevenagel condensation reactions, Microp Mesop Mater, 263 (2018) 173-180.
[21] X. Zeng, X. Xiao, J. Chen, H. Wang, Electron-hole interactions in choline-phosphotungstic acid boosting molecular oxygen activation for fuel desulfurization, Appl Catal B-Environ, 248 (2019) 573-586.
[22] S. Damyanova, J.L.G. Fierro, Surface properties of titania-supported 12-molybdophosphoric acid hydrodesulphurization catalysts, Appl Catal A-Gen, 144 (1996) 59-77.
[23] P. Cruz, M. Fajardo, I. del Hierro, Y. Pérez, Selective oxidation of thioanisole by titanium complexes immobilized on mesoporous silica nanoparticles: elucidating the environment of titanium(iv) species, Catal Sci Technol, 9 (2019) 620-633.
[24] J. Ortiz-Bustos, M. Fajardo, I. del Hierro, Y. Pérez, Versatile titanium dioxide nanoparticles prepared by surface-grown polymerization of polyethylenimine for photodegradation and catalytic CC bond forming reactions, Mol. Catal., 475 (2019) 110501.
[25] Z. Yu, D. Wang, S. Xun, M. He, R. Ma, W. Jiang, H. Li, W. Zhu, H. Li, Amorphous TiO2-supported Keggin-type ionic liquid catalyst catalytic oxidation of dibenzothiophene in diesel, Petrol. Sci., 15 (2018) 870-881.
[26] A. Pacuła, K. Pamin, J. Kryściak-Czerwenka, Z. Olejniczak, B. Gil, E. Bielańska, R. Dula, E.M. Serwicka, A. Drelinkiewicz, Physicochemical and catalytic properties of hybrid catalysts derived from 12-molybdophosphoric acid and montmorillonites, Appl. Catal. A-Gen., 498 (2015) 192-204.
[27] A. Duan, G. Wan, Z. Zhao, C. Xu, Y. Zheng, Y. Zhang, T. Dou, X. Bao, K. Chung, Characterization and activity of Mo supported catalysts for diesel deep hydrodesulphurization, Catal. Today, 119 (2007) 13-18.
[28] J.B. Black, N.J. Clayden, P.L. Gai, J.D. Scott, E.M. Serwicka, J.B. Goodenough, Acrolein oxidation over 12-molybdophosphates: I. Characterization of the catalyst, J. Catal., 106 (1987) 1-15.
[29] Y. Tian, G. Wang, J. Long, J. Cui, W. Jin, D. Zeng, Ultra-deep oxidative desulfurization of fuel with H2O2 catalyzed by phosphomolybdic acid supported on silica, Chinese J. Catal., 37 (2016) 2098-2105.
[30] T.-h. Chang, NMR characterization of the supported 12-heteropoly acids, J. Chem. Soc. Faraday Trans., 91 (1995) 375-379.
[31] K. Narasimharao, B.H. Babu, N. Lingaiah, P.S.S. Prasad, S.A. Al-Thabaiti, Ammoxidation of 2-methyl pyrazine on supported ammonium salt of 12-molybdophosphoric acid catalysts: The influence of nature of support, J. Chem. Sci., 126 (2014) 487-498.

[32] P.G. Vázquez, M.N. Blanco, C.V. Cáceres, Catalysts based on supported 12-molybdophosphoric acid, Catal. Lett., 60 (1999) 205-215.
[33] A.a. Concellón, P. Vázquez, M. Blanco, C. Cáceres, Molybdophosphoric Acid Adsorption on Titania from Ethanol–Water Solutions, J. Colloid Interface Sci., 204 (1998) 256-267.
[34] M. Sadakane, E. Steckhan, Electrochemical Properties of Polyoxometalates as Electrocatalysts, Chem. Rev., 98 (1998) 219-238.
[35] S.S. Kale, U. Armbruster, R. Eckelt, U. Bentrup, S.B. Umbarkar, M.K. Dongare, A. Martin, Understanding the role of Keggin type heteropolyacid catalysts for glycerol acetylation using toluene as an entrainer, Appl Catal A-Gen, 527 (2016) 9-18.
[36] E.I. García-López, G. Marcì, I. Krivtsov, J. Casado Espina, L.F. Liotta, A. Serrano, Local Structure of Supported Keggin and Wells–Dawson Heteropolyacids and Its Influence on the Catalytic Activity, J Phys Chem C, 123 (2019) 19513-19527.
[37] M.N. Hossain, H.C. Park, H.S. Choi, A Comprehensive Review on Catalytic Oxidative Desulfurization of Liquid Fuel Oil, Catalysts, 9 (2019) 229.
[38] P. Cruz, E.-A. Granados, M. Fajardo, I. del Hierro, Y. Pérez, Heterogeneous oxidative desulfurization catalysed by titanium grafted mesoporous silica nanoparticles containing tethered hydrophobic ionic liquid: A dual activation mechanism, Appl. Catal. A-Gen., 587 (2019) 117241.
[39] A.A. Tsyganenko, E.N. Storozheva, O.V. Manoilova, T. Lesage, M. Daturi, J.C. Lavalley, Brønsted acidity of silica silanol groups induced by adsorption of acids, Catal. Lett., 70 (2000) 159-163.
[40] A. Akopyan, E. Eseva, P. Polikarpova, A. Kedalo, A. Vutolkina, A. Glotov, Deep Oxidative Desulfurization of Fuels in the Presence of Brönsted Acidic Polyoxometalate-Based Ionic Liquids, Molecules, 25 (2020) 536.
[41] H. Taghiyar, B. Yadollahi, Keggin polyoxometalates encapsulated in molybdenum-iron-type Keplerate nanoball as efficient and cost-effective catalysts in the oxidative desulfurization of sulfides, Sci. Total Environ., 708 (2020) 134860.
[42] M.A. Rezvani, S. Khandan, Synthesis and characterization of new sandwich-type polyoxometalate/nanoceramic nanocomposite, Fe2W18Fe4@FeTiO3, as a highly efficient heterogeneous nanocatalyst for desulfurization of fuel, Solid State Sci, 98 (2019) 106036.
[43] H. Shi, Y. Yu, Y. Zhang, X. Feng, X. Zhao, H. Tan, S.U. Khan, Y. Li, E. Wang, Polyoxometalate/TiO2/Ag composite nanofibers with enhanced photocatalytic performance under visible light, Appl. Catal. B: Environ. 221 (2018) 280-289.
[44] Y. Gao, L. Cheng, R. Gao, G. Hu, J. Zhao, Deep desulfurization of fuels using supported ionic liquid-polyoxometalate hybrid as catalyst: A comparison of different types of ionic liquids, J. Hazard. Mater., 401 (2021) 123267.
[45] S. Zhang, G. Zhao, S. Gao, Z. Xi, J. Xu, Secondary alcohols oxidation with hydrogen peroxide catalyzed by [n-C16H33N(CH3)3]3PW12O40: Transform-and-retransform process between catalytic precursor and catalytic activity species, J. Mol. Catal. A-Chem. 289 (2008) 22-27.
[46] Z.P. Pai, Y.A. Chesalov, P.V. Berdnikova, E.A. Uslamin, D.Y. Yushchenko, Y.V. Uchenova, T.B. Khlebnikova, V.P. Baltakhinov, D.I. Kochubey, V.I. Bukhtiyarov, Tungsten Peroxopolyoxo Complexes as Advanced Catalysts for the Oxidation of Organic Compounds with Hydrogen Peroxide, Appl. Catal. A-Gen. 604 (2020) 117786.